**Smart Structures and Systems**, *Vol. 20, No. 2 (2017) 151-162*
DOI: https://doi.org/10.12989/sss.2017.20.2.151


# Development of a double-sliding friction damper (DSFD)

Shaodong Shen[1a], Peng Pan[*1,2], Jiangbo Sun[1b], Runhua Gong[1c], Haishen Wang[1d] and Wei Li[1e]

[1]*Department of Civil Engineering, Tsinghua University, Beijing 100084, China*
[2]*Key Laboratory of Civil Engineering Safety and Durability of China Education Ministry, Tsinghua University, Beijing 100084, China*

*(Received December 28, 2016, Revised March 30, 2017, Accepted April 7, 2017)*

**Abstract.** In practical engineering, the friction damper is a widely used energy dissipation device because of its large deformation capacity, stable energy dissipation capability, and cost effectiveness. While based on conventional friction dampers, the double-sliding friction damper (DSFD) being proposed is different in that it features two sliding friction forces, i.e., small and large sliding friction forces, rather than a single-sliding friction force of ordinary friction dampers. The DSFD starts to deform when the force sustained exceeds the small-sliding friction force, and stops deforming when the deformation reaches a certain value. If the force sustained exceeds the large sliding friction force, it continues to deform. Such a double-sliding behavior is expected to endow structures equipped with the DSFD better performance in both small and large earthquakes. The configuration and working mechanism of the DSFD is described and analyzed. Quasi-static loading tests and finite element analyses were conducted to investigate its hysteretic behavior. Finally, time history analysis of the single-degree-of-freedom (SDOF) and multi-degree-of-freedom (MDOF) systems were performed to investigate the seismic performance of DSFD-equipped structures. For the purpose of comparison, tests on systems equipped with conventional friction dampers were also performed. The proposed DSFD can be realized perfectly, and the DSFD-equipped structures provide better performances than those equipped with conventional friction dampers in terms of interstory drift and floor acceleration. In particular, for the MDOF system, the DSFD helps the structural system to have a uniform distributed interstory drift.

**Keywords:** friction damper; double-sliding; quasi-static test; finite element modeling; time history analysis

## 1. Introduction

The development of the friction damper began in the late 1970s. Through the action of friction during the relative sliding between two contacting surfaces, the friction damper transforms the building's vibration energy into thermal energy for absorption, enabling a strong dissipation of energy and stable structural response, as well as providing a cost-effective implementation. In addition, its friction force can be easily determined by adjusting the magnitude of the preload, so it has a wide range of engineering applications. To adapt to different types of building structures, researchers around the world have developed a variety of friction dampers. Pall and Marsh (1982) proposed a Pall-type friction damper. This is a two-way friction damper mounted in the center of the X-brace that achieves energy dissipation using sliding friction generated by a friction brake pad at the brace intersection through the tension and deformation from compression of the chain bar. Compared with conventional friction dampers, the friction of the Pall friction damper is more stable and its hysteretic behavior is not affected by buckling forces of the supporting members (Lefferts *et al.* 1982). Ohnishi *et al.* (1999) developed a steel tube friction damper that dissipates energy by sliding friction between a tightly fitted steel bar and a mold tube, which exhibits good energy dissipation performance. Morgen and Kurama (2004) proposed a frictional rotational energy dissipation node designed for unbonded post-tensioned prestressed reinforced-concrete beam-to-column joints. The test results show that the energy dissipation nodes can effectively improve the energy dissipation capacity of the beam-column joints, achieving stable energy dissipation performance. To have torsional vibration damping and energy dissipation, Shirkhani *et al.* (2015) proposed a splint rotational friction damper for a steel frame and demonstrated that it could effectively reduce the displacement response of the steel frame under earthquake excitation and improve its seismic performance.

To date, most of the friction dampers have only a single sliding force. It is difficult to take into account the energy dissipation needs for small and large earthquakes simultaneously. Specifically, if the friction damper has a large sliding friction force, it can slide during large earthquakes, but not necessarily slide during small earthquakes and thus providing only stiffness but no energy dissipation for the structure. Conversely, if the sliding friction is small, the friction damper can slide and dissipate energy during small earthquakes, but it may not have large

*Corresponding author, Professor
E-mail: panpeng@mail.tsinghua.edu.cn
[a] Ph.D. Student
E-mail: ssd15@mails.tsinghua.edu.cn
[b] Engineer
[c] MSc Student
[d] MSc Student
[e] MSc Student



ISSN: 1738-1584 (Print), 1738-1991 (Online)

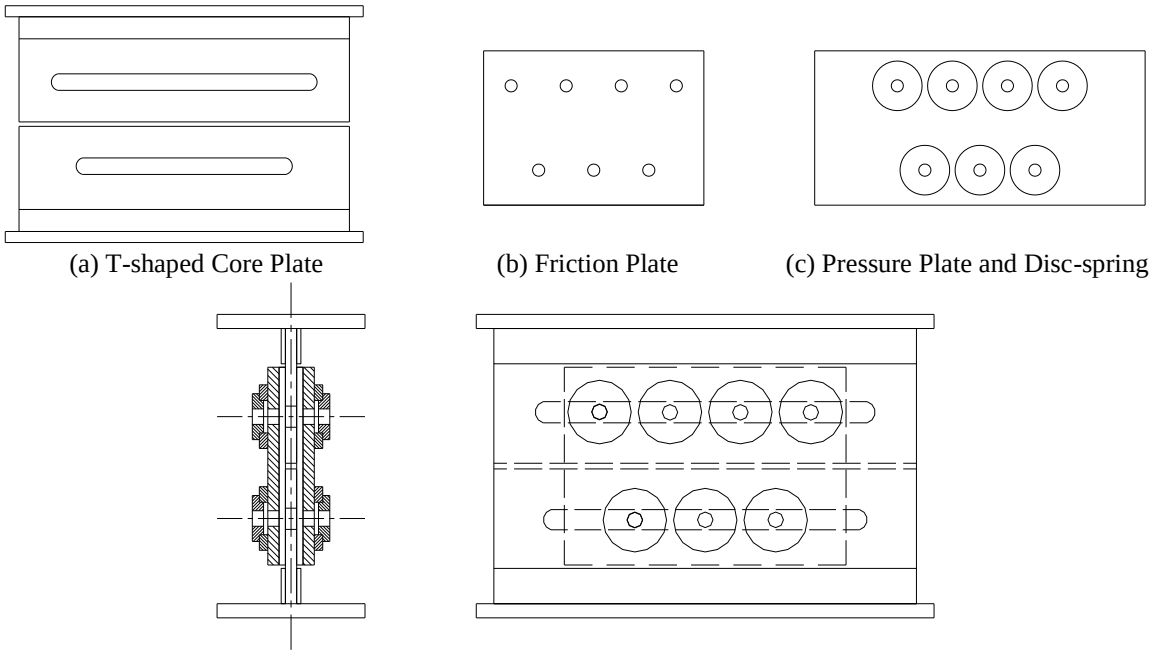

(a) T-shaped Core Plate (b) Friction Plate (c) Pressure Plate and Disc-spring

(d) Assembly

Fig. 1 Configuration of the double sliding friction damper (DSFD)

enough energy dissipation capacity during large earthquakes. To this end, some effort has gone into adjusting sliding friction forces of friction dampers using intelligent control technology. Chen et al. studied the seismic response control of the structure installed with a piezoelectric variable friction damper and achieved good results (Chen *et al*. 2004, Chen and Chen 2003). However, such friction dampers are complex in construction and expensive in application.

A novel friction damper with low cost, simple structure is proposed that features two levels of sliding each producing a sliding friction force, Referred to as the double-sliding friction damper (DSFD), it is expected to overcome limitations in a conventional friction dampers with its single sliding friction force. For small earthquakes, it can achieve sliding against a relative smaller friction force and dissipates some energy but can also slide against a much larger friction force and dissipation more energy during large earthquakes, endowing the damper a satisfactory controlled seismic response. In this paper, the configuration and working mechanism of the DSFD is outlined. Quasi-static loading tests and finite element analyses that were conducted to investigate its hysteretic behavior are described. Finally, time history analysis of a single-degree-of-freedom (SDOF) and a multi-degree-of-freedom (MDOF) systems were performed to investigate the seismic performance of DSFD-equipped structures.

## 2. Configuration of DSFD

The DSFD belongs to a band-type shearing class of friction damper (Fig. 1). It mainly consists of two T-shaped core plates, two friction plates, two pressure plates, some disc springs and high-strength bolt groups. The upper and lower T-shaped core plates are separated by a gap which allows a relative displacement in the horizontal direction, that enables shear displacement for energy dissipation. Both core plates are slotted, and the slot length determines the allowable sliding distance of the core plate. The friction plates are made of a material that provides a stable coefficient of friction. The two front and back plates are in contact with the upper and lower T-shaped core plates. Hence sliding friction occurs when the T-core plate and the friction plate are moving relative to each other. The front and back pressure plates are both made of stainless steel that are bonded to the front and back friction plates, respectively. The disc springs and high strength bolt groups are used to exert pressure on the pressure plate. The pressure is transmitted to the contact surface between the friction and core plates. Because of the disc spring, the pressure on the pressure plates is rather stable. The upper row of disc springs and bolt groups determine the sliding force required for the movement of the upper T-shaped core plate, and the lower row of disc springs and bolt groups determine the sliding force of the lower T-shaped core plate. Note that the sliding force can be easily adjusted by changing the number of discs and bolt groups and/or the pressure exerted by each disc and bolt group.

In the DSFD, the total pressure force exerted by the lower row of springs and bolt groups than that exerted by the upper row. Therefore, the sliding force of the lower T-shaped core plate is smaller than that of the upper T-shaped core plate. The sliding of the former is expected to start first during small earthquakes. As stated earlier, the sliding distance is limited by the size of the slots on the lower T-shaped core plates. When the sliding distance of the lower T-shaped core plate reaches the limit, the lower T-shaped

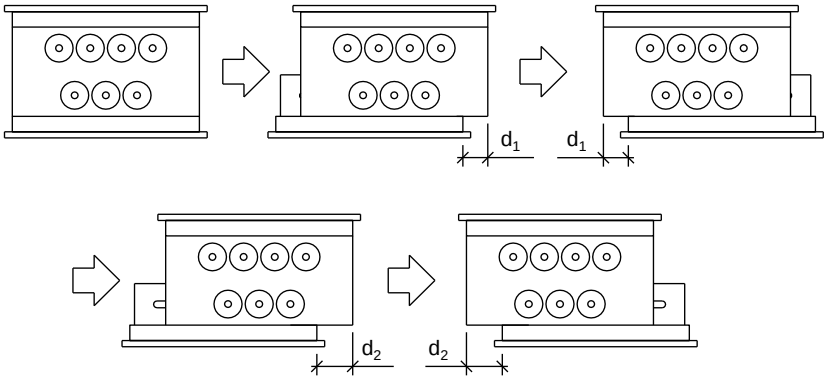


(a) Deformation pattern of DSFD

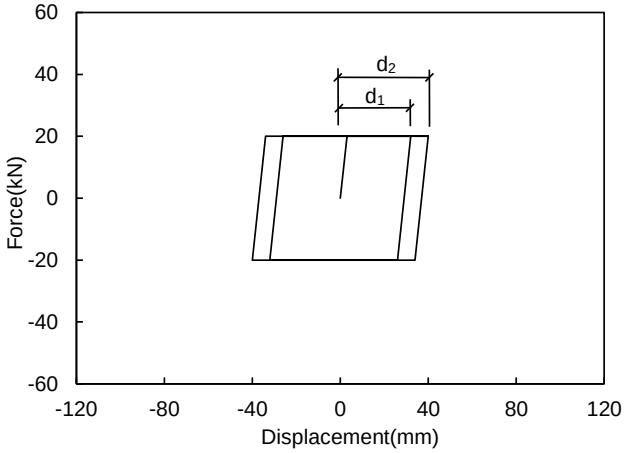


(b) Hysteretic curve of DSFD

Fig. 2 Behavior of the DSFD under small earthquakes

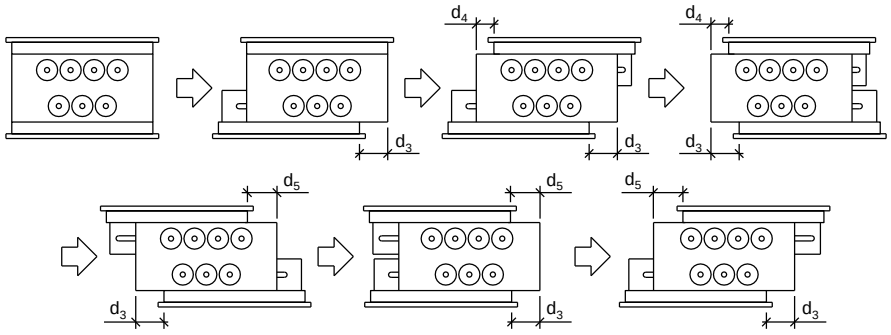


(a) Deformation pattern of DSFD

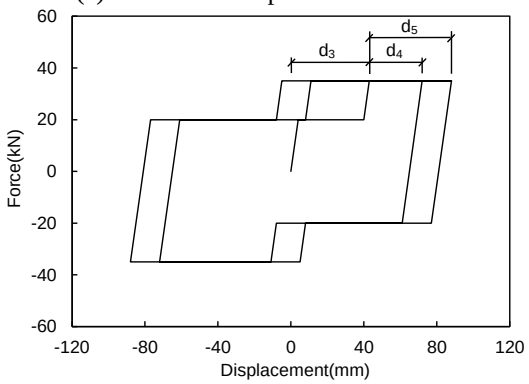


(b) Hysteretic curve of DSFD

Fig. 3 Behavior of the DSFD under large earthquakes

core plate stops sliding. If the force sustained by the DSFD further increases to a certain value, which is expected to happen in large earthquakes, the upper T-shaped core plate begins to slide. In this way, a two stage sliding is achieved.

Fig. 2 shows a schematic diagram of the working mechanism of DSFD and its idealized hysteretic curve corresponding to small earthquakes (Lee *et al*. 2016). For small earthquakes, the displacement amplitude of the damper does not always exceed the displacement limit of the lower T-shaped core plate. Specifically, $d_1$ and $d_2$ (Fig. 2) do not exceed the displacement limit. Therefore, for a small earthquake, the upper core plate rarely starts to slide; only the damper slides in first-order friction to dissipate energy. Hence the working mechanism and hysteresis curve characteristics of the DSFD for small earthquakes are similar to those of conventional friction dampers.

In regard to the working mechanism and hysteresis curve of the DSFD during large earthquakes (Fig. 3) exhibit a two-stage deformation. When the movement of the lower core plate reaches its maximum limit $d_3$, the upper core plate starts to slide until the damper begins to sustain reverse displacement. For displacements in the opposite direction, the sliding friction force of the lower T-shaped core plate equals that of the smaller one until the damper moving in the opposite direction reaches the displacement limit $d_3$, and then the upper core plate starts sliding. In this way, a more complex hysteresis curve develops (Fig. 3(b)).

## 3. Test and simulation of DSFD

### *3.1 Quasi-static test of DSFD*

Quasi-static tests were conducted to investigate the behavior of the DSFD. The test setup [Fig. 4(a)] mainly includes a hydraulic servo actuator, loading frame, and displacement transducer. With the loading frame bolt-anchored to the ground, the actuator acts on the upper beam of the loading frame, and the specimen are connected to the upper and lower beams of the loading frame, so that the shear displacement of the specimen could be generated horizontally. A displacement transducer was installed between the upper and lower connecting plate of the specimen. The displacement transducer has a range of ±100 mm to a precision of 0.01 mm; the specimen deformation can be accurately measured (Ye *et al.* 2016a, b).

Fig. 4(b) shows a photo of the test specimen. As mentioned before, the sliding friction force can be set by adjusting the pressure force on each ][disc spring high strength bolt group. The first level of sliding friction force was set to 19 kN, and the corresponding displacement limit was set to 40 mm. The second level of sliding friction force was 35 kN. Depending on cross-section and material properties, the lateral stiffness of the specimen is about 60000 kN/m.

Displacement control was applied to the quasi-static loading of the specimen (Deng et al., 2015). The loading scheme (Fig. 5) is divided into two stages, one a displacement of amplitude 36 mm for 4 cycles, and the other of amplitude 72 mm for 7 cycles. The respective stages of loading are deformations of the DSFD active in small and large earthquakes.

The displacement-shear force relationship of the specimen (Fig. 6) shows first a cyclic deformation with amplitude of 36 mm. When the loading displacement increases to 72 mm, the specimen first slid to the displacement limit of 40 mm under the first sliding force of 19 kN, and then friction force starts to increase to 35 kN, namely the second level of sliding friction force.

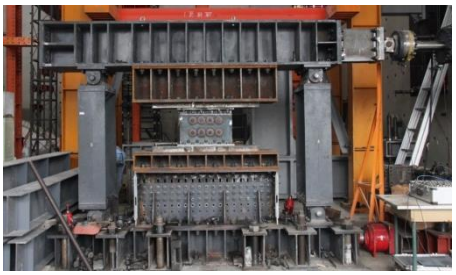

(a) Test setup

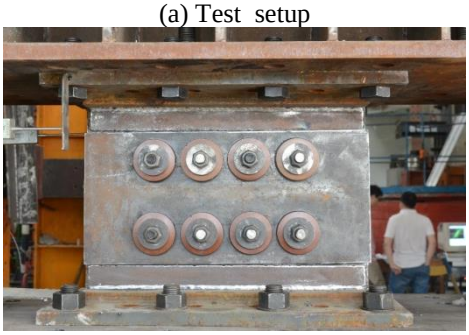

(b) Specimen

Fig. 4 Test setup and test specimen

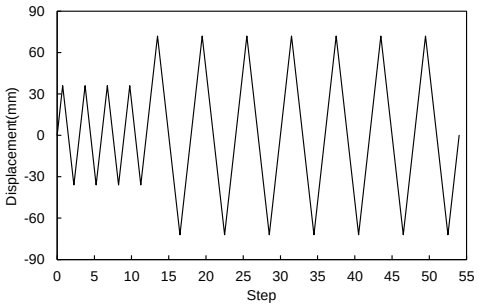


Fig. 5 Loading scheme for the quasi-static test

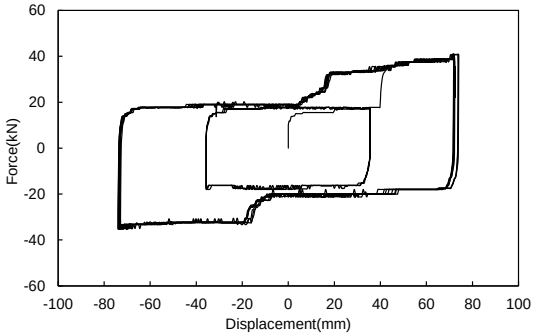


Fig. 6 Displacement–force relationship of the DSFD

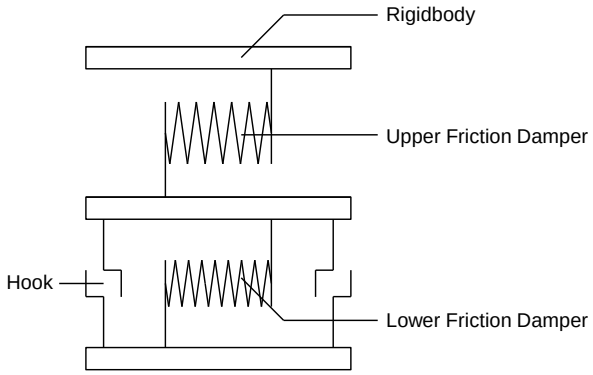


Fig. 7 Modeling of the DSFD

Subsequently, under both sliding friction, the specimen dissipates the energy. Also, note that when the displacement amplitude switches to 72 mm, the area of the hysteresis loop for the damper increases significantly, implying that the energy dissipation capacity of the damper also is greatly enhanced. Based on observations from tests, it can be conclude that the DSFD configuration executes the double-sliding friction mechanism as specified.

### *3.2 Molding and simulation of DSFD*

The DSFD can be modeled by a two friction components connected in series (Fig. 7). Both components can deformed in the horizontal direction. The lower friction component has relatively small sliding friction force, and the upper friction component has a relatively large sliding friction force. Each of the components is represented by a nonlinear spring with a bilinear hysteresis behavior. Two hook elements are connected in parallel to the spring representing the lower friction component. These two hook elements are to ensure that the lower conventional friction component only deforms in an allowable range.

The expected hysteresis curves of the DSFD (Fig. 8) exhibits a two-stage deformation. The first stage of deformation features a large initial stiffness, the first level of sliding friction force, and an almost zero second stiffness. The second stage of deformation features a large third stiffness, which is identical to the initial stiffness, a second level of sliding friction force, and an almost zero fourth stiffness. The unloading stiffness equals the initial stiffness. For the purpose of comparison, hysteresis curves are plotted for two conventional friction dampers, designated FD-L and FD-S, having sliding friction forces equal to those of the first and second levels, respectively. The initial stiffnesses for both conventional dampers are identical with that of the DSFD, and the second stiffness is almost zero.

The finite-element model of the specimen (Fig. 4(b)) was established using a general finite element analysis program called SAP2000 (Beijing Civil King Software Technology Company Limited 2012), and the analyses were performed using a specified loading scheme (Fig. 5). Hysteresis curves of the specimen obtained from analysis and from physical tests were compared (Fig. 9); essentially both results agree well. However, a notable difference in regard to the third stiffness of the DSFD is apparent. This is because the stiffness in contact is assumed to be infinite in the numerical model but is not the case in physical tests. Nevertheless, the finite element method simulates the behavior of the DSFD quite accurately, and can be used to characterize the dynamic behavior of the DSFD (Downey *et al.* 2016).

## 4. Effects of DSFD on the SDOF system

### *4.1 SDOF system equipped with DSFD*

Nonlinear time-history analyses were conducted to investigate the effects of the DSFD on the seismic response of structures. In this section, a single-degree-of-freedom (SDOF) system is studied. The lateral stiffness of the SDOF system is about 11800 kN/m and the weight is about 470 kN (Fig. 10(a)). The friction damper was modeled as a substructure attached to the main structure by a rigid beam with hinges at both ends (Fig. 10(b)). Three types of friction dampers providing three distinct models were considered. The first model is the SDOF system equipped with a conventional friction damper with relatively large sliding friction force, i.e., FD-L.

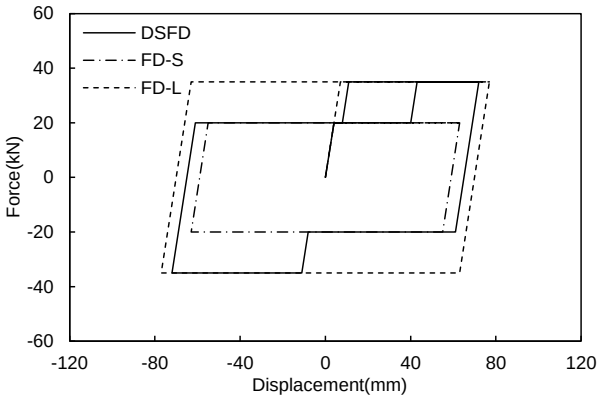


Fig. 8 Hysteresis curves of three dampers

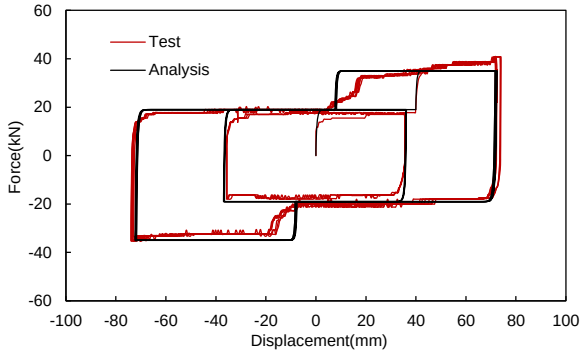


Fig. 9 Comparison of hysteresis curves between test and analysis

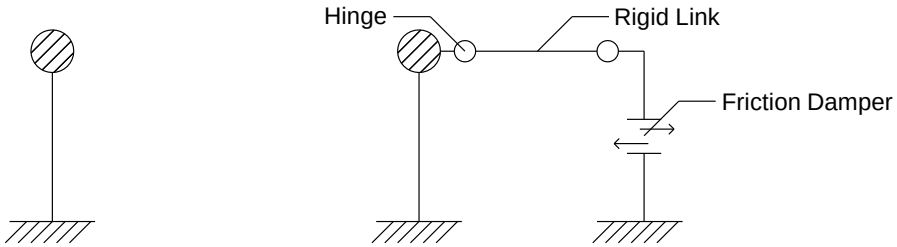


Fig. 10 Finite element analysis model for the SDOF system (right) with and (left) without dampers

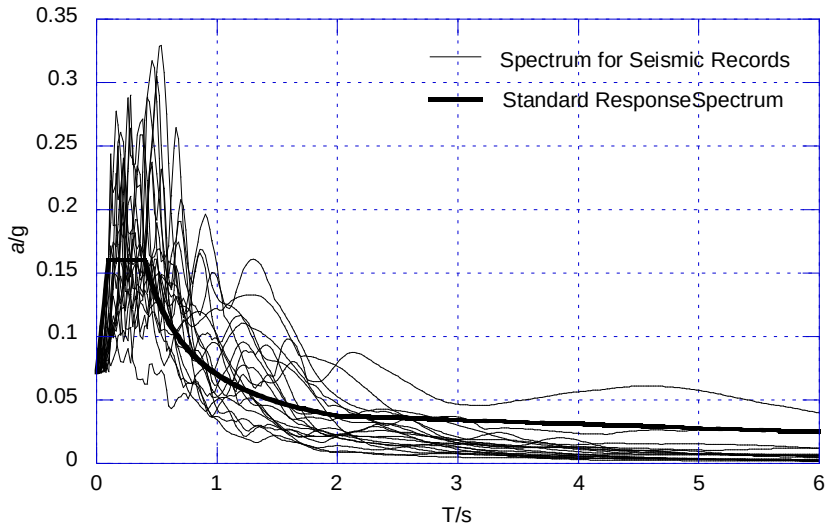


(a) Response spectra for small earthquakes

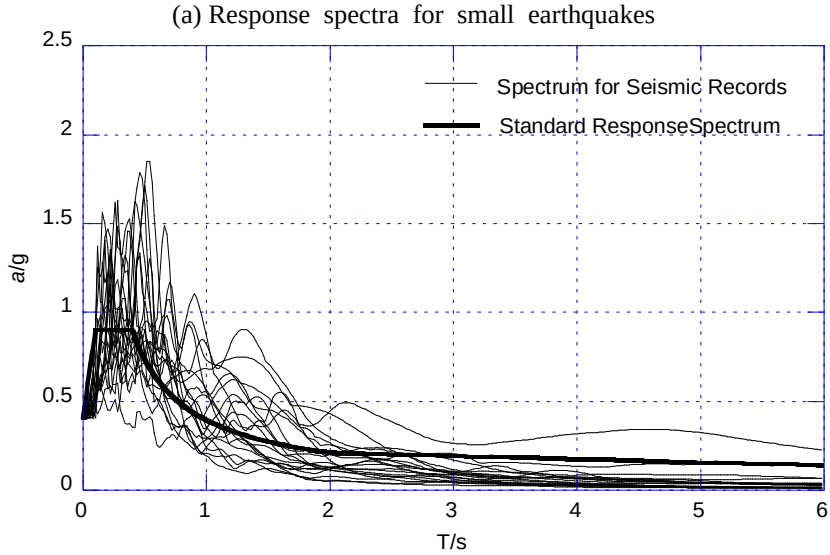


(b) Response spectra for large earthquakes

Fig. 11 Response spectra for 22 ground motions recommended in the report FEMA P695

The initial stiffness of FD-L is 6930 kN/m, which is about 37% of the total lateral stiffness of the structure system. The sliding friction force of FD-L is 60 kN. The second model is the SDOF system equipped with a relatively small sliding friction force, i.e., FD-S. FD-S has the same stiffness as FD-L, but its sliding friction force is only 20 kN. The third model is the SDOF system equipped with a DSFD. The DSFD has a first-level sliding friction force of 20 kN and a second-level of 60 kN, which are identical with the sliding friction forces of FD-S and FD-L, respectively. The three dampers have identical initial lateral stiffness.

Adopted for this study was a sequence of ground motions consisting of 22 far-field records recommended in the report FEMA P695 (FEMA 2009) for collapse vulnerability analyses. The noise signal of the 22 far-field records was removed to guarantee the accuracy of the analysis results (Yi *et al*. 2012 and 2013).

Table 1 Maximum interstory drift for the SDOF system under small earthquakes (units: mm)

| | Ground motion | SDOF without damper | SDOF with FD-L | SDOF with FD-S | SDOF with DSFD |
|---|---|---|---|---|---|
| 1 | Northridge (Beverly Hills-Mulhol) | 10.8 | 4.31 | 4.62 | 4.55 |
| 2 | Northridge (Canyon Country-WLC) | 7.46 | 5.67 | 5.63 | 5.66 |
| 3 | Duzce | 5.65 | 3.89 | 4.03 | 4.01 |
| 4 | Hector Mine | 10.7 | 5.26 | 5.27 | 5.27 |
| 5 | Imperial Valley (Delta) | 5.68 | 3.43 | 3.56 | 3.57 |
| 6 | Imperial Valley (EI Centro Array#11) | 6.62 | 5.65 | 4.99 | 4.96 |
| 7 | Kobe (Nishi-Akashi) | 13.3 | 4.33 | 4.92 | 4.73 |
| 8 | Kobe (Shin-Osaka) | 7.10 | 4.61 | 4.72 | 4.78 |
| 9 | Kocaeli(Duzce) | 7.58 | 7.81 | 7.76 | 7.65 |
| 10 | Kocaeli (Arcelik) | 3.60 | 1.82 | 1.89 | 1.89 |
| 11 | Landers (Yermo Fire Station) | 5.91 | 4.03 | 3.73 | 3.89 |
| 12 | Landers (Coolwater) | 10.7 | 6.51 | 5.89 | 5.91 |
| 13 | Loma Prieta (Capitola) | 8.47 | 7.39 | 6.73 | 6.61 |
| 14 | Loma Prieta (Gilroy Array#3) | 6.52 | 4.41 | 4.59 | 4.54 |
| 15 | Manjil | 6.35 | 4.89 | 4.75 | 4.76 |
| 16 | Superstition Hills (EI Centro Imp. Co.) | 5.95 | 3.19 | 3.30 | 3.37 |
| 17 | Superstition Hills (Poe Road) | 10.3 | 3.73 | 4.01 | 3.96 |
| 18 | Cape Mendocino | 12.8 | 5.07 | 6.16 | 5.92 |
| 19 | Chi-Chi (CHY101) | 6.03 | 4.37 | 5.01 | 4.94 |
| 20 | Chi-Chi (TCU045) | 5.98 | 3.59 | 3.91 | 3.87 |
| 21 | San Fernando | 5.49 | 5.61 | 4.90 | 4.85 |
| 22 | Friuli | 5.75 | 4.98 | 4.99 | 4.96 |
| | Mean value | 7.67 | 4.75 | 4.79 | 4.76 |
| | Standard Deviation | 2.61 | 1.37 | 1.24 | 1.2 |
| | 84 Percentile | 10.28 | 6.12 | 6.03 | 5.96 |

According to China Building Seismic Design Code GB50011-2010, the peak ground acceleration (PGA) of the ground motions were adjusted to 70 gal and 400 gal for small and large earthquakes, respectively; the response spectra to ground motions were plotted for both (Fig. 11(a) and 11(b)), respectively]. For the purpose of comparison, the design spectra are also given in the figures. The spectra of the ground motions were found to agree statistically with the design spectra.

Table 2 Maximum interstory drift of the SDOF system under large earthquakes (units: mm)

| | Ground motion | SDOF without damper | SDOF with FD-L | SDOF with FD-S | SDOF with DSFD |
|---|---|---|---|---|---|
| 1 | Northridge (Beverly Hills-Mulhol) | 61.6 | 33.5 | 49.9 | 34.4 |
| 2 | Northridge (Canyon Country-WLC) | 42.6 | 31.8 | 35.1 | 31.7 |
| 3 | Duzce | 32.2 | 25.0 | 28.7 | 24.6 |
| 4 | Hector Mine | 60.7 | 33.6 | 49.5 | 33.8 |
| 5 | Imperial Valley (Delta) | 32.4 | 19.9 | 25.4 | 19.5 |
| 6 | Imperial Valley (EI Centro Array#11) | 37.9 | 28.7 | 28.2 | 26.9 |
| 7 | Kobe (Nishi-Akashi) | 76.2 | 39.8 | 60.6 | 40.0 |
| 8 | Kobe (Shin-Osaka) | 40.5 | 27.2 | 34.6 | 27.5 |
| 9 | Kocaeli (Duzce) | 43.3 | 43.7 | 37.9 | 42.5 |
| 10 | Kocaeli (Arcelik) | 20.6 | 10.4 | 11.1 | 10.7 |
| 11 | Landers (Yermo Fire Station) | 33.7 | 24.2 | 29.9 | 25.0 |
| 12 | Landers (Coolwater) | 60.9 | 37.9 | 49.9 | 37.6 |
| 13 | Loma Prieta (Capitola) | 48.3 | 38.9 | 42.4 | 38.8 |
| 14 | Loma Prieta (Gilroy Array#3) | 37.3 | 27.1 | 29.7 | 27.3 |
| 15 | Manjil | 36.3 | 28.0 | 31.3 | 28.3 |
| 16 | Superstition Hills (EI Centro Imp. Co.) | 33.9 | 19.1 | 27.0 | 20.9 |
| 17 | Superstition Hills (Poe Road) | 58.7 | 26.3 | 45.9 | 27.6 |
| 18 | Cape Mendocino | 73.4 | 47.8 | 62.9 | 48.7 |
| 19 | Chi-Chi (CHY101) | 34.6 | 31.4 | 32.8 | 31.2 |
| 20 | Chi-Chi (TCU045) | 34.2 | 25.3 | 31.9 | 26.9 |
| 21 | San Fernando | 31.3 | 23.5 | 27.2 | 23.6 |
| 22 | Friuli | 32.9 | 29.0 | 29.7 | 28.8 |
| | Mean value | 43.8 | 29.64 | 36.44 | 29.83 |
| | Standard Deviation | 14.9 | 8.547 | 12.36 | 8.401 |
| | 84 Percentile | 58.70 | 38.19 | 48.80 | 38.23 |

### *4.2 Effects of DSFD on interstory drift*

Time history analyses were conducted, and the responses of interstory drift and horizontal floor acceleration were obtained. Note that the interstory drift equals the top displacement for the SDOF system. Table 1 compares the maximum interstory drift for the 22 ground motions, the PGAs of which were adjusted to 70 cm/s$^2$. Compared with the model with no damper, those equipped with friction dampers showed notably smaller interstory

drifts for most earthquakes. The mean value of the interstory drifts is 4.75 mm for the DSFD-equipped model, which is similar to those of the models equipped with FD-L and FD-S. The standard deviation of the interstory drift is about 1.20 mm for the DSFD-equipped model, which is smaller than those for the FD-L and FD-S-equipped models.

The sum of the mean and standard deviation, which is commonly called the 84 percentile is also given in the table. The 84 percentile of the interstory drift for the DSFD-equipped model is the smallest of the three. The conclusion is that the DSFD performs slightly better than the other two friction dampers in term of interstory drift control for small earthquakes. The maximum interstory drift of the four models is summarized in Table 2 for large earthquakes. The mean value of the interstory drift is 29.64 mm, 36.44 mm, and 29.83 mm for the models equipped with FD-L, FD-S, and DSFD, respectively. The 84 percentile of the interstory drift is 38.19 mm, 48.80 mm, and 38.23 mm for these models. The models equipped with DSFD and FD-L produced much smaller mean values, standard deviations, and 84 percentiles than the FD-S- equipped model, indicating that DSFD executes similar control as FD-L, but much better control than FD-S for large earthquakes.

### *4.3 Effects of DSFD on floor acceleration*

Floor acceleration is important to maintain the functionality of building structures, thus effects of DSFD on floor acceleration were investigated and the effects of the three dampers in controlling floor acceleration during small earthquake were compared (see Table 3). The mean value and 84 percentile of the floor acceleration are 1.27 m/s$^2$ and 1.61 m/s$^2$ for the DSFD-equipped model, which are similar to the respective values for the FD-S-equipped model, but significantly smaller than those for the FD-L-equipped model. Similarly, the effects of the three dampers in controlling floor acceleration during large earthquakes were also compared (see Table 4). The mean value and 84 percentile of the floor acceleration are 6.59 m/s$^2$ and 8.45 m/s$^2$ for the DSFD-equipped model, which is similar to the respective values for the FD-L-equipped model, but significantly smaller than that for the FD-S-equipped model. Hence DSFD performs better in controlling floor acceleration than FD-L for smaller earthquakes, and FD-S for large earthquakes.

In summary, as for the SDOF system, DSFD exhibited more satisfactory control than conventional friction dampers for both interstory drift and floor acceleration. It is as good as FD-S for small earthquakes, and as good as FD-L for large earthquakes. The conventional friction dampers, FD-L and FD-S, can execute satisfactory control only during large and small earthquakes, respectively. Combining the responses is particularly beneficial because the DSFD initiates sliding and dissipates energy during small earthquakes like FD-S and provides large energy dissipation capability during large earthquakes like FD-L. In contrast, FD-L remains "locked" and dissipates little energy in small earthquakes, and FD-S dissipates little energy in large earthquakes.

Table 3 Maximum floor acceleration of the SDOF system under small earthquakes (units: m/s$^2$)

| | Ground motion | SDOF without damper | SDOF with FD-L | SDOF with FD-S | SDOF with DSFD |
|---|---|---|---|---|---|
| 1 | Northridge (Beverly Hills-Mulhol) | 1.89 | 1.13 | 1.02 | 1.02 |
| 2 | Northridge (Canyon Country-WLC) | 1.73 | 1.96 | 1.61 | 1.62 |
| 3 | Duzce | 1.01 | 1.09 | 0.98 | 0.99 |
| 4 | Hector Mine | 2.05 | 1.52 | 1.26 | 1.26 |
| 5 | Imperial Valley (Delta) | 1.11 | 1.13 | 0.91 | 0.96 |
| 6 | Imperial Valley (EI Centro Array#11) | 1.59 | 2.17 | 1.75 | 1.75 |
| 7 | Kobe (Nishi-Akashi) | 2.63 | 1.93 | 1.16 | 1.12 |
| 8 | Kobe (Shin-Osaka) | 1.14 | 1.18 | 0.94 | 0.97 |
| 9 | Kocaeli (Duzce) | 1.45 | 2.14 | 1.76 | 1.82 |
| 10 | Kocaeli (Arcelik) | 0.88 | 1.00 | 0.94 | 0.95 |
| 11 | Landers (Yermo Fire Station) | 1.04 | 1.06 | 0.88 | 0.90 |
| 12 | Landers (Coolwater) | 2.05 | 2.15 | 1.58 | 1.58 |
| 13 | Loma Prieta(Capitola) | 2.12 | 2.41 | 1.80 | 1.76 |
| 14 | Loma Prieta (Gilroy Array#3) | 1.83 | 1.92 | 1.68 | 1.67 |
| 15 | Manjil | 1.85 | 1.71 | 1.53 | 1.51 |
| 16 | Superstition Hil ls (EI Centro Imp. Co.) | 1.19 | 1.14 | 0.98 | 0.99 |
| 17 | Superstition Hills (Poe Road) | 2.01 | 1.32 | 0.89 | 0.89 |
| 18 | Cape Mendocino | 2.81 | 2.62 | 1.56 | 1.53 |
| 19 | Chi-Chi(CHY101) | 1.29 | 1.21 | 0.96 | 0.96 |
| 20 | Chi-Chi(TCU045) | 1.31 | 1.39 | 0.90 | 0.93 |
| 21 | San Fernando | 1.86 | 1.83 | 1.44 | 1.43 |
| 22 | Friuli | 1.46 | 1.63 | 1.39 | 1.40 |
| | Mean value | 1.65 | 1.62 | 1.27 | 1.27 |
| | Standard Deviation | 0.517 | 0.49 | 0.34 | 0.34 |
| | 84 Percentile | 2.17 | 2.11 | 1.61 | 1.61 |

Table 4 Maximum floor acceleration of the SDOF system under large earthquakes (units: m/s$^2$)

| | Ground motion | SDOF without damper | SDOF with FD-L | SDOF with FD-S | SDOF with DSFD |
|---|---|---|---|---|---|
| 1 | Northridge (Beverly Hills-Mulhol) | 10.8 | 5.69 | 8.06 | 5.73 |
| 2 | Northridge (Canyon Country-WLC) | 9.88 | 7.73 | 7.80 | 7.75 |
| 3 | Duzce | 5.77 | 4.95 | 4.94 | 5.00 |
| 4 | Hector Mine | 11.7 | 6.85 | 9.09 | 7.07 |
| 5 | Imperial Valley (Delta) | 6.34 | 4.01 | 4.28 | 4.05 |
| 6 | Imperial Valley (EI Centro Array#11) | 9.82 | 8.99 | 8.39 | 8.64 |
| 7 | Kobe (Nishi-Akashi) | 15.0 | 7.32 | 11.07 | 7.61 |
| 8 | Kobe (Shin-Osaka) | 5.95 | 4.54 | 4.62 | 4.65 |
| 9 | Kocaeli (Duzce) | 8.21 | 8.57 | 7.29 | 8.65 |
| 10 | Kocaeli (Arcelik) | 5.02 | 4.72 | 3.32 | 3.57 |
| 11 | Landers (Yermo Fire Station) | 5.92 | 4.26 | 4.30 | 4.28 |
| 12 | Landers (Coolwater) | 11.8 | 7.13 | 8.83 | 7.16 |
| 13 | Loma Prieta(Capitola) | 12.1 | 9.17 | 9.99 | 9.26 |
| 14 | Loma Prieta (Gilroy Array#3) | 10.5 | 8.63 | 8.93 | 8.75 |
| 15 | Manjil | 10.6 | 8.16 | 8.84 | 8.32 |
| 16 | Superstition Hills (EI Centro Imp. Co.) | 6.80 | 4.99 | 5.95 | 5.47 |
| 17 | Superstition Hills (Poe Road) | 11.5 | 5.06 | 8.21 | 5.37 |
| 18 | Cape Mendocino | 16.1 | 10.2 | 12.69 | 9.42 |
| 19 | Chi-Chi(CHY101) | 7.45 | 4.52 | 5.53 | 4.66 |
| 20 | Chi-Chi(TCU045) | 7.50 | 4.64 | 6.11 | 4.97 |
| 21 | San Fernando | 10.6 | 7.38 | 9.00 | 7.53 |
| 22 | Friuli | 8.32 | 7.10 | 7.17 | 7.10 |
| | Mean value | 9.44 | 6.57 | 7.47 | 6.59 |
| | Standard Deviation | 2.99 | 1.90 | 2.38 | 1.86 |
| | 84 Percentile | 12.43 | 8.47 | 9.85 | 8.45 |

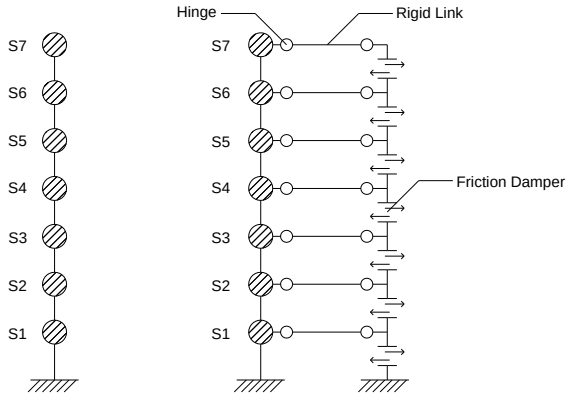


Fig. 12 Modeling of the MDOF system (left) without and (right) with dampers

## 5. Effects of DSFD on MDOF System

### *5.1 MDOF System Equipped with DSFD*

To investigate the effects of DSFD on MDOF system, a seven-story stick model consisting of a shear spring and masses was constructed (Fig. 12(a)). The mass of each floor, represented by a concentrated mass, was 730000 kg. The story stiffness of 1$^{st}$ to 3$^{rd}$ story, 4$^{th}$ to 6$^{th}$ story, and 7$^{th}$ story was 39000, 33000, and 29000 kN/m, respectively. Friction dampers equipped in each story were modeled as a substructure (Fig. 12(b)). The substructure was connected with the main structure by a rigid beam with hinges at both ends, so that dampers could work in the corresponding story.

With this model, three scenarios were conducted using the three types of friction dampers. In the first scenario, each floor was equipped with a FD-L, accounting for 37% of the lateral stiffness of the story, and the sliding force was 1950 kN. For the second scenario, each floor was equipped with a FD-S and had the same parameter values as the first model, except for the sliding force of 650 kN. In the third scenario, each floor was installed with a DSFD, which had a first sliding force of 650 kN and a second sliding force of 1,950 kN. The stiffness of DSFD is identical with that of FD-L and FD-S. Time history analyses were performed to investigate the effectiveness of DSFD, using the same group of ground motions introduced in the above section. Similarly, both small and large earthquakes were considered with the PGA set to 70 gal and 400 gal, respectively.

### *5.2 Effects of DSFD on interstory drift*

From the effects of DSFD for the small earthquakes (Fig. 13), the mean value and the 84 percentile of the maximum interstory drift ratio among the three models equipped with FD-L, FD-S, and DSFD showed that the DSFD-equipped model has the smallest interstory drift ratio, i.e., 1/595, indicating that the control effects of the DSFD on the interstory drift is satisfactory for small earthquakes. For large earthquakes (Fig. 14), the mean value and the 84 percentile of maximum drift ratio for the three models show the maximum interstory drift angle commonly occurs at the bottom story for large earthquakes. This is easy to

understand as the seismic force sustained by the bottom story is the largest. The DSFD-equipped model shows a similar performance as that with FD-L equipped in terms of controlling the interstory drift angle for large earthquakes.

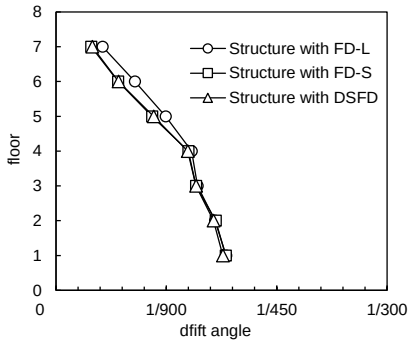


(a) Mean value

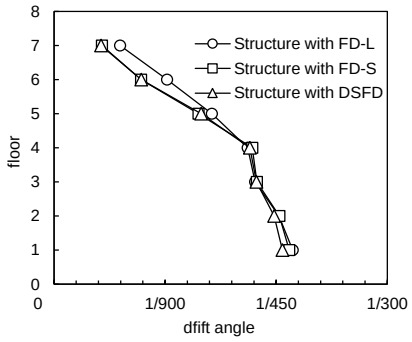


(b) 84 percentile

Fig. 13 Interstory drift angle for small earthquakes

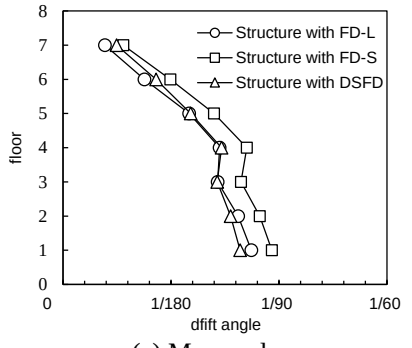


(a) Mean value

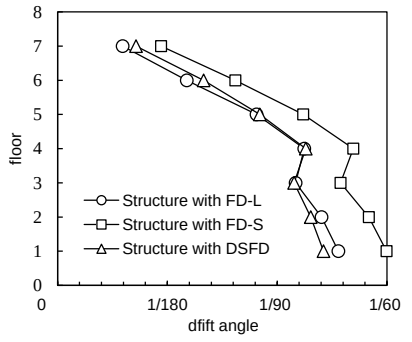


(b) 84 percentile

Fig. 14 Interstory drift angle for large earthquakes

Table 5 DCF of the MDOF system for small and large earthquakes

| Model | Small earthquakes | Large earthquakes |
|---|---|---|
| MDOF with FD-S | 1.49 | 1.35 |
| MDOF with FD-L | 1.42 | 1.43 |
| MDOF with DSFD | 1.47 | 1.33 |

The distribution of interstory drift angle is important in preventing collapses of structures under large earthquakes, and commonly a uniform distribution is preferred. To reflect the concentration of structural interstory drift quantitatively, the deformation concentration factor (*DCF*) is used (Pan *et al.* 2015). *DCF* is defined as the ratio of the maximum interstory drift angle to the overall deformation angle, which can be calculated as Eq. (1).

$$DCF = \max\{d_i / h_i\}/(\Delta / \Sigma h_i) \quad (1)$$

where $d_i$ is the inter-story displacement of the $i$-th story, $h_i$ is the height of the $i$-th story, and $\Delta$ is the roof displacement. A *DCF* of 1.0 means a completely uniform distribution; a large *DCF* implies a soft-story mechanism.

The results of *DCF* for the models are given in Table 5. For small earthquakes, *DCF* for the model equipped with DSFD is 1.474, which is smaller than that of the FD-S-equipped model, but larger than that of the FD-L-equipped model. This is mainly because FD-L does not slide in small earthquakes, and the model equipped with FD-L remains elastic, whereas both FD-S and DSFD models slide, and have some stiffness degradation at some stories. However, for large earthquakes, DSFD shows notable advantages. The *DCF* of the DSFD-equipped model is 1.33, which is the smallest of the three. This is because in large earthquakes, all dampers slides. For FD-L and FD-S, once the damper slides, the story stiffness degrades and cannot recover, whereas for DSFD, the story stiffness can recover once the story drift reaches a specific value, and deformation occurs to the stories which has relatively small deformations, leading finally to a uniform distributed interstory drift angle.

### *5.3 Effects of DSFD on floor acceleration*

To investigate the distribution of floor acceleration for MDOF systems, the mean floor accelerations are summarized in Figs. 15 and 16 for small and large earthquakes, respectively. From Fig. 15, the FD-S model shows significant advantage in controlling floor acceleration. Both the mean value and 84 percentile of the floor acceleration response are only about 80% of that of the structure equipped with FD-L. DSFD achieves good performance as for FD-S during small earthquakes. However, in large earthquakes, the observation is different. From Fig. 16, both the mean value and the 84 percentile of the floor acceleration for the FD-S model is about 110% of the respective value for the FD-L model. In this case, the DSFD model achieves good performance like the FD-L model. Based on these results, DSFD exhibits very adequate floor acceleration control for both small and large earthquakes.

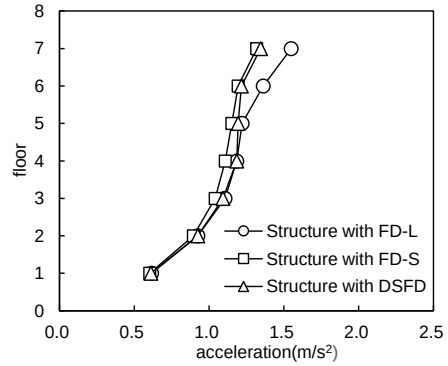


(a) Mean value

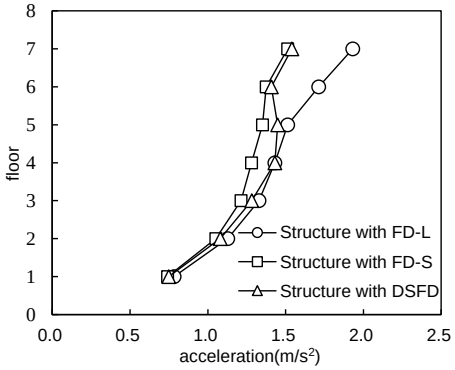


(b) 84 percentile

Fig. 15 Floor acceleration for small earthquakes

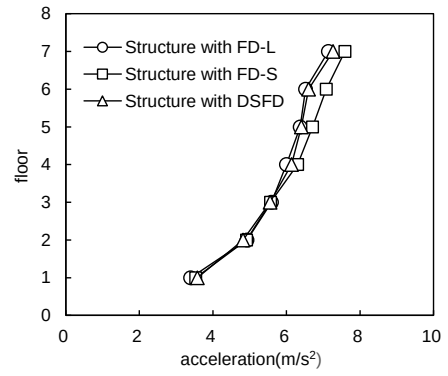


(a) Mean value

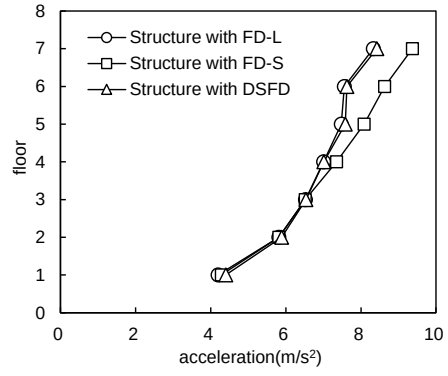


(b) 84 percentile

Fig. 16 Floor acceleration for large earthquakes

## 6. Conclusions

A double-sliding force friction damper (DSFD) was proposed and under testing was able to dissipate energy effectively during both small and large ground motion simulations. Quasi-static loading test and finite element analyses were performed to investigate hysteretic behavior. Time history analysis of SDOF and MDOF systems were performed to investigate the seismic performance of DSFD-equipped structures. For the purpose of comparison, systems equipped with conventional friction dampers were also conducted. The main conclusions obtained in this study are as follows:

- The proposed DSFD with its rather simple structure function successfully as specified.
- The finite element model was able to simulate the behavior of the DSFD accurately.
- The effective control by DSFD on the interstory drift angle and floor acceleration is similar to FD-S (FD-L), which has a sliding force identical to the first (second) level sliding force of DSFD.
- For the MDOF system under large earthquakes, DSFD is able to distribute the interstory drift angle more uniformly.

## Acknowledgments

The financial support from the state key research project in 13th Five-Year under grant no. 2016YFC0701901-2, the Beijing Science and Technology Program under grant no. Z161100001216015, and the Natural Science Foundation of China under grants no. 51422809 and 51578314 is gratefully acknowledged.

## References

Beijing Civil King Software Technology Company Limited (2012), *SAP2000 Chinese Version Using Guide*, 2nd Ed., China Communication Press, Beijing, China. (in Chinese).

Chen, G. and Chen, C.Q. (2003), "Semi-active control of a steel frame with Piezoelectric friction dampers", *Proceeding of the SPIE 5057, Smart Structures and Materials 2003: Smart Systems and Nondestructive Evaluation for Civil Infrastructures*, 207-217, San Diego, California, August.

Chen, G.D., Garrett, G.T., Chen, C.Q. and Cheng, F.Y. (2004), "Piezoelectric friction dampers for earthquake mitigation of buildings: design, fabrication, and characterization", *Struct. Eng. Mech.*, **17**(3-4), 539-556.

Deng, K.L., Pan, P., Nie, X., Xu, X.G., Feng, P. and Ye, L.P. (2015), "Study of GFRP Steel Buckling Restraint Braces", *J. Composi. Constr.*, **19**(6), 04015009:1-8.

Downey, A., Cao, L., Laflamme, S., Taylor, D. and Rides, J. (2016), "High capacity variable friction damper based on band brake technology", *Eng. Struct.*, **113**, 287-298.

FEMA (2009), "Quantification of building seismic performance factors", *FEMA P695*, Federal Emergency Management Agency, Washington, DC, California, USA.

Gur, S., Mishra, S.K. and Roy, K. (2016), "Stochastic seismic response of building with super-elastic damper with super-elastic damper", *Mech. Syst. Signal Pr.*, 72-73, 642-659.

Hosseini, M., Fekri, M. and Yekrangnia, M.(2016). "Seismic

performance of an innovative structural system having seesaw motion and columns equipped with friction dampers at base level", *Struct. Des. Tall Spec. Build.*, **25**, 842-865.

Lee, C.H., Kim, J., Kim, D.H., Ryu, J. and Ju, Y.K. (2016), "Numerical and experimental analysis of combined behavior of shear-type friction damper and non-uniform strip damper for multi-level seismic protection", *Eng. Struct.*, **114**, 75-92.

Lefferts, E.J., Markley, F.L. and Shuster, M.D. (1982), "Kalman filtering for spacecraft attitude estimation", *J. Guid. Control Dynam.*, **5**(5), 417-429.

Mazza, F. (2016), "Nonlinear seismic analysis of r.c. framed buildings with setbacks retrofitted by damped braces", *Eng. Struct.*, **126**, 559-570.

Miguel, L.F.F., Miguel, L.F.F. and Lopez, R.H. (2015). "Simultaneous optimization of force and placement of friction dampers under seismic loading", *Eng. Optimiz.*, **48**(4), 582-602.

Morgen, B.G. and Kurama, Y.C. (2004), "A Friction Damper for Post-Tensioned Precast Concrete Beam-To-Column Joints", *Proceedings of the 13th World Conference on Earthquake Engineering*, paper No.3189, Vancouver, B.C., Canada, August.

Ohnishi, H., Kitajima, K., Nakanishi, M. and Adachi, H. (1999), "A study on friction dampers for response-control retrofit of existing R/C buildings", *Transactions of the JCI*, **21**, 439-446.

Pall, A.S. and Marsh, C. (1982), "Response of friction damped braced frames", *J. Struct. Div. - ASCE*, **108**(6),1313-1323.

Pan, P., Wu, S.J. and Nie, X. (2015), "A distributed parameter model of a frame pin-supported wall structure", *Earthquake Engineering & Structural Dynamic*, **44**, 1643-1659.

Shirkhani, A., Mualla, I.H., Shabakhty, N. and Mousavi, S.R. (2015), "Behavior of steel frames with rotational friction dampers by endurance time method", *J. Constr. Steel Res.*, **107**, 211-222.

Ye, X.W., Dong, C.Z. and Liu, T.(2016a), "Image-based structural dynamic displacement measurement using different multi-object tracking algorithms", *Smart Struct. Syst.*, **17**(6), 935-956.

Ye, X.W., Su, Y.H., Xi, P.S., Chen, B. and Han, J.P. (2016b), "Statistical analysis and probabilistic modeling of WIM monitoring data of an instrumented arch bridge", *Smart Struct. Syst.*, **17**(6), 1087-1105.

Yi, T.H., Li, H.N. and Sun, H.M. (2013), "Multi- stage structural damage diagnosis method based on 'energy-damage' theory", *Smart Struct. Syst.*, **12**(3-4), 345-361.

Yi, T.H., Li, H.N. and Zhao, X.Y. (2012), "Noise smoothing for structural vibration test signals using an improved wavelet thresholding technique", *Sensors*, **12**(8), 11205-11220.